LONGITUDINAL BEAM INSTABILITY IN SSMB LASER MODULATORS: A CAVITY MODE DECOMPOSITION APPROACH

Y. Dai*, T. Li, Z. Liu, X. Deng, L. Yan, Tsinghua University, Beijing, China

Abstract

Steady-state microbunching (SSMB) is a promising mechanism for generating high-average-power coherent radiation by maintaining microbunches in a storage ring. In an SSMB laser modulator (LM), the interaction between electron bunches and the recirculating coherent undulator radiation can drive longitudinal beam instabilities, which may limit the overall performance. In this work, we investigate the longitudinal single-bunch multi-turn instability using a cavity mode decomposition approach. The evolution of the longitudinal wakefield is derived by expanding the radiation into a complete set of cavity eigenmodes, accurately capturing the optical evolution of the field over multiple turns. Based on the derived wakefields, the longitudinal beam dynamics equations are formulated to analyze the instability growth rates. Numerical simulations show excellent agreement with the theoretical model, validating the mode decomposition technique. These findings provide critical insights into the instability characteristics and suggest effective mitigation strategies for the design and operation of SSMB storage rings.

INTRODUCTION

In 2010, Ratner and Chao proposed the concept of steady-state microbunching (SSMB) to generate high-average-power coherent radiation in storage rings [1]. In an SSMB storage ring, the conventional radiofrequency (RF) cavity is replaced by a laser modulator (LM) system, which generally comprises an undulator and a laser cavity, as schematically illustrated in Fig. 1. When the electron beam traverses the undulator, it oscillates and is modulated by the laser field, enabling microbunching at optical wavelengths. However, the emitted undulator radiation will bounce and evolve within the cavity. The interaction between the beam and the radiation may trigger longitudinal beam instabilities, degrading the performance of the storage ring [2–6].

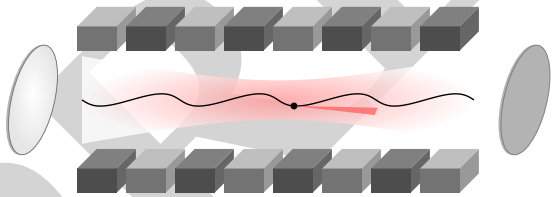

Figure 1: Laser modulator.

To account for the recirculating nature of radiation within the optical cavity, the cavity properties, such as diffraction and mirror-induced focusing, must be considered. In this work we adopt a mode-decomposition approach. By expanding the radiation into a complete set of cavity eigenmodes, we are able to represent the global evolution of the radiation as the sum of individual mode components. This approach provides further insights into the LM instability characteristics of SSMB storage rings. More details of this work can be found in Ref. [7].

* dyj24@mails.tsinghua.edu.cn

CAVITY MODE DECOMPOSITION

Hermite–Gaussian Modes

In the optical cavity, the envelope $u(\boldsymbol{r})$ of a laser field with frequency ω and wavenumber $k = \omega/c$ propagating along the z-axis satisfies the paraxial wave equation. In Cartesian coordinates, the solutions are the Hermite–Gaussian modes [8]:

$$E_{mn} = E_0 \frac{w_0}{w(z)} H_m\left(\frac{\sqrt{2}x}{w(z)}\right) H_n\left(\frac{\sqrt{2}y}{w(z)}\right) \exp\left(-\frac{x^2+y^2}{w^2(z)}\right) \times \exp\left[-\mathrm{i}\frac{k(x^2+y^2)}{2R(z)} + \mathrm{i}(m+n+1)\psi(z) - \mathrm{i}kz\right], \tag{1}$$

where E_0 is the amplitude normalization constant, H_m and H_n are Hermite polynomials, $w(z) = w_0\sqrt{1+(z/z_\mathrm{R})^2}$ is the beam waist, $R(z) = z + z_\mathrm{R}^2/z$ is the radius of curvature of the wavefront, $\psi(z) = \arctan(z/z_\mathrm{R})$ is the Gouy phase, and $z_\mathrm{R} = \pi w_0^2/\lambda$ is the Rayleigh length.

Mode Decomposition of Undulator Radiation

By completeness, any paraxial field can be expanded in terms of Hermite–Gaussian modes:

$$\boldsymbol{E}(\boldsymbol{r}) = \sum_{mn} C_{mn}\boldsymbol{E}_{mn}(\boldsymbol{r}), \tag{2}$$

the excitation of mode coefficient ΔC_{mn} by a moving electron with velocity $\boldsymbol{v}$ is proportional to the work done by the mode field on the electron along its trajectory $\boldsymbol{r}(t)$ [9]. The energy spectrum of the radiation of the mode is given by the Parseval theorem:

$$\frac{\mathrm{d}W_{mn}}{\mathrm{d}\omega} = \frac{e^2}{8\pi P_{mn}}\left|\int_{-\infty}^{+\infty} \boldsymbol{v}\cdot\boldsymbol{E}^*_{mn}(\boldsymbol{r})\,\mathrm{e}^{-\mathrm{i}\omega t}\,\mathrm{d}t\right|^2, \tag{3}$$

where P_{mn} is the power normalization constant of the mode [9, Eq. (4)]. The Hermite–Gaussian mode components of the undulator radiation are shown in Fig. 2 with the parameters in Table 1.

For planar undulators, due to the absence of electron motion along the y-axis, only the even-n modes with x-polarization (σ-mode) and odd-n modes with y-polarization

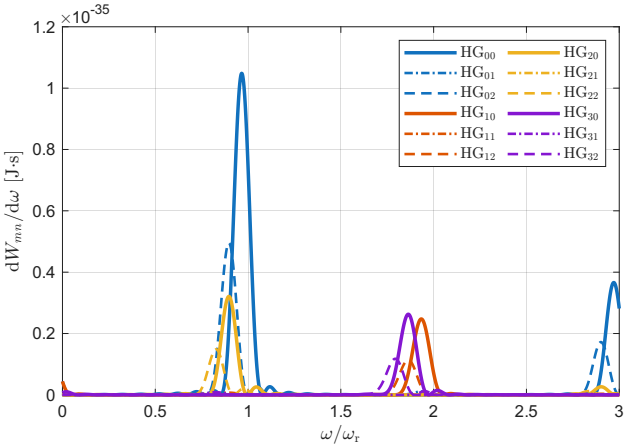

Figure 2: Hermite–Gaussian mode components of undulator radiation. Different line colors are for different m, and different line styles are for different n. The odd-n modes is much weaker than the even-n modes.

(π-mode) are excited, and the π-mode radiation is much weaker than the σ-mode radiation. The peaks of the mode spectrum are around the harmonics of the fundamental resonant frequency ω_r. While the fundamental mode (HG_{00}) is the strongest mode, high-order modes with $m, n > 0$ also contribute significantly to the total radiation spectrum, especially for higher harmonics.

MULTI-TURN WAKEFIELD EVOLUTION

The electromagnetic interaction between the beam and its environment is described by the radiation impedance and wakefield. For a single electron, the real part of the impedance $\mathrm{Re}[Z_\parallel(\omega)]$ is directly proportional to the radiation spectrum [10, 11]. In free space, the longitudinal wake function is the inverse cosine transform of the real part of the impedance $W_\parallel(z) = \mathcal{F}^{-1}_{\cos}[Z_\parallel](z)$ when $z > 0$, where [10, 11]

$$\mathcal{F}^{-1}_{\cos}[Z_\parallel](z) := \frac{2}{\pi}\int_0^{+\infty} \mathrm{Re}[Z_\parallel(\omega)]\cos(kz)\,\mathrm{d}\omega. \quad (4)$$

In the cavity, however, the frequency spectrum is discrete due to the resonance condition. For a cavity with two identical mirrors, the resonance frequencies are [12]:

$$\omega_{mnq} = \frac{c}{L}(\psi_{mn} + \pi q), \quad (5)$$

where L is the cavity length, $\psi_{mn} = (m + n + 1)\arccos(1 - L/R)$ is the transverse phase shift introduced by the Gouy phase, R is the radius of curvature (ROC) of the cavity mirrors, and $q = 1, 2, 3, \ldots$ is the longitudinal mode index. Thus the integral in Eq. (4) should be replaced by series:

$$W_\parallel(z) = \frac{2}{\pi}\sum_{mnq} \mathrm{Re}[Z_{\parallel mn}(\omega_{mnq})]\cos(k_{mnq}z)\Delta\omega_{\mathrm{FSR}}, \quad (6)$$

where $\mathrm{Re}[Z_{\parallel mn}]$ is the impedance of HG_{mn} mode, $k_{mnq} = \omega_{mnq}/c$ is the wavenumber of the mode, and $\Delta\omega_{\mathrm{FSR}} = \omega_{mn(q+1)} - \omega_{mnq} = \pi c/L$ is the free spectral range. In the short-range regime where $z \ll L$, the discrete series of $W_\parallel(z)$ asymptotically approaches the continuous integral $\mathcal{F}^{-1}_{\cos}[Z_\parallel](z)$ in Eq. (4), which can be denoted as:

$$W_\parallel(z) \simeq \mathcal{F}^{-1}_{\cos}[Z_\parallel](z), \quad z \ll L. \quad (7)$$

In the long-range regime where $z \sim L$, conversely, the discreteness becomes manifest. For SSMB applications, we only focus on the local properties of the wakefield on multiple round-trips, i. e. shifting the coordinate from z to $(z + 2pL)$, where integer $p = 0, 1, 2, \ldots$ is the number of round-trips and the local coordinate $z \ll L$, then the asymptotic behavior in the short-range regime gives:

$$W_\parallel(z + 2pL) \simeq \sum_{mn}\Big[\cos(2p\psi_{mn})\,\mathcal{F}^{-1}_{\cos}[Z_{\parallel mn}](z) - \sin(2p\psi_{mn})\,\mathcal{F}^{-1}_{\sin}[Z_{\parallel mn}](z)\Big]. \quad (8)$$

Therefore, the evolution of the wakefield is determined by the superposition of all modes with different phase shift ψ_{mn}. Figure 3 shows the evolution of the wakefield $W_\parallel(z + 2pL)$ over round-trips with the parameters in Table 1. In contrast to the short-range wakefield $W_\parallel(z)$ strictly constrained to $z > 0$ due to causality, the long-range wakefield $W_\parallel(z+2pL)$ exhibits a non-zero distribution for both positive and negative z.

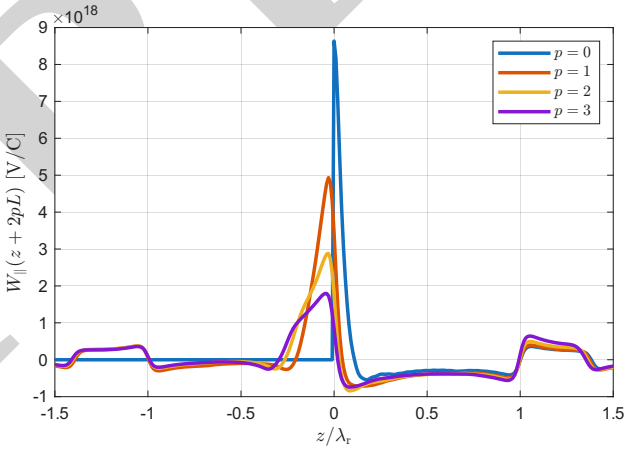

Figure 3: Evolution of the wakefield $W_\parallel(z+2pL)$. The blue, orange, yellow, and purple lines represent the wakefield after zero ($p = 0$), one ($p = 1$), two ($p = 2$), and three ($p = 3$) round-trip(s) within the cavity, respectively. Here the phase shift $\psi_{00} = 0.01$ to show a small evolution.

BEAM DYNAMICS AND INSTABILITY

Longitudinal Dynamics Equations

For simplicity here we only consider one macroparticle representing the entire microbunch consisting of N_e electrons. The longitudinal coordinates of the macroparticle in the j-th turn are denoted as (z_j, δ_j), where z_j is the longitudinal position relative to the reference particle and

$\delta_j = \gamma_j/\gamma_0 - 1$ is the relative energy deviation. The longitudinal dynamics equations are:

$$z_{j+1} = z_j + R_{56}\delta_{j+1}, \tag{9a}$$

$$\delta_{j+1} = \delta_j + \frac{eV_\mathrm{L}}{E_0}\sin(k_\mathrm{L} z_j) + \Delta\delta_j, \tag{9b}$$

where R_{56} is the longitudinal dispersion strength, V_L and k_L are the effective voltage and wavenumber of the laser in the modulator, and $\Delta\delta_j$ is the energy deviation change due to the interaction with the undulator radiation field [7]:

$$\Delta\delta_j = -\frac{N_\mathrm{e}W_\mathrm{u}}{E_0} - \frac{N_\mathrm{e}e^2}{E_0}\sum_{p=1}^{j} W_\parallel(z_{j-p} - z_j + pC), \tag{10}$$

where C is the circumference of the storage ring. The first term W_u represents the energy loss due to the spontaneous radiation emitted by the bunch itself; the second term $W_\parallel(z_{j-p} - z_j + pC)$ represents the energy modulation due to the stimulated radiation from the previous turns. To ensure the phase-locking condition, the revolution time C/c of electron beams in the storage ring is designed to be an integer multiple of the round-trip time $2L/c$ of laser in the cavity, which is exactly our case of Eq. (8).

Growth Rate of Instability

The linearized beam dynamics around the equilibrium point gives the growth rate of instability [7]:

$$\frac{1}{\tau} = \frac{N_\mathrm{e}e^2cR_{56}}{2\mu_0 E_0 C}\sum_{p=1}^{\infty} W'_\parallel(pC)\sin(p\mu_0), \tag{11}$$

where $\mu_0 = \sqrt{-hR_{56}}$ is the synchrotron oscillation frequency, and $h = eV_\mathrm{L}k_\mathrm{L}/E_0$ is the energy chirp strength. The superposition of all modes gives the total growth rate, which exhibits a complex resonance structure with multiple peaks and valleys as a function of the tune μ_0 [7, Fig. 13].

SIMULATION AND DISCUSSION

As an example, we simulate the dynamics with parameters listed in Table 1 [13].

Table 1: Parameters for an SSMB Example

Symbol	Value	Description
E_0	250 MeV	Beam energy
λ_L	1064 nm	Modulation laser wavelength
K	1.76	Undulator parameter
h	5000 m^{-1}	Energy chirp strength
N_u	10	Number of undulator periods
L_u	2 m	Undulator length
L	4 m	Cavity length
R	2.26 m	ROC of cavity mirrors
z_R	0.72 m	Rayleigh length
C	48 m	Storage ring circumference
R_{56}	−10 µm	Storage ring dispersion

Under small electron number, the longitudinal coordinate z_j could be well fitted by a sinusoidal function of turn number j. Figure 4 shows good agreement between the growth rate fitted from the simulation results and the theoretical growth rate calculated by Eq. (11).

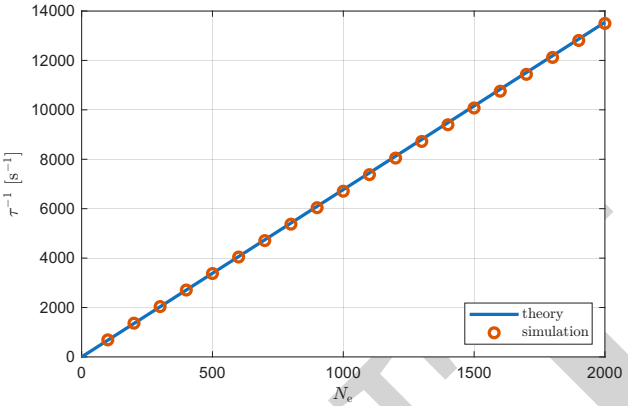

Figure 4: Growth rate with different electron number N_e. Blue line refers to the theoretical growth rate calculated by Eq. (11), and orange dots refer to the growth rate fitted from the simulation results.

Finally, it should be emphasized that the convergence of high-order cavity modes is relatively slow, with the fundamental mode accounting for only a fraction of the total contribution. Consequently, high-order modes exert a significant influence on the instability. In the practical design of laser cavities for SSMB, various techniques such as the implementation of D-shaped mirrors are typically employed to accelerate the attenuation of these high-order modes by introducing mode-selective losses [14]. Such measures serve as an effective means to suppress the instabilities induced by high-order transverse modes. Futher details in this respect are expected to be discussed in our later work.

SUMMARY

In this paper, we have established a comprehensive theoretical and numerical framework to investigate the longitudinal beam instabilities driven by coherent undulator radiation within the LM of an SSMB storage ring. By expanding the radiation field into a complete set of Hermite-Gaussian modes, the evolution of the wakefields within the optical cavity is accurately captured, revealing the complex interplay between different modes and their contributions to the instability growth rates. Our work provides insights into the LM instability and mitigation strategies for the design and operation of SSMB storage rings.

ACKNOWLEDGMENTS

This work is supported by the National Key Research and Development Program of China (No. 2022YFA1603403), the Beijing Outstanding Young Scientist Program (No. JWZQ20240101006), the National Natural Science Foundation of China (NSFC No. 12522512, 124B2104), and Tsinghua University Dushi Program.

REFERENCES

[1] D. F. Ratner and A. W. Chao, "Steady-state microbunching in a storage ring for generating coherent radiation", *Phys. Rev. Lett.*, vol. 105, no. 15, p. 154801, 2010. doi:10.1103/PhysRevLett.105.154801

[2] C.-Y. Tsai, A. W. Chao, Y. Jiao, H.-W. Luo, M. Ying, and Q. Zhou, "Coherent-radiation-induced longitudinal single-pass beam breakup instability of a steady-state microbunch train in an undulator", *Phys. Rev. Accel. Beams*, vol. 24, no. 11, p. 114401, 2021. doi:10.1103/PhysRevAccelBeams.24.114401

[3] C.-Y. Tsai, "Longitudinal single-bunch instabilities driven by coherent undulator radiation in the cavity modulator of a steady-state microbunching storage ring", *Nuclear Instruments and Methods in Physics Research Section A: Accelerators, Spectrometers, Detectors and Associated Equipment*, vol. 1042, p. 167454, 2022. doi:10.1016/j.nima.2022.167454

[4] C.-Y. Tsai, "Theoretical formulation of multiturn collective dynamics in a laser cavity modulator with comparison to robinson and high-gain free-electron laser instability", *Phys. Rev. Accel. Beams*, vol. 25, no. 6, p. 064401, 2022. doi:10.1103/PhysRevAccelBeams.25.064401

[5] C.-Y. Tsai and X. Deng, "Simple model for electron beam dynamics in laser modulators and radiation characteristics of steady-state microbunching storage ring", *Phys. Rev. Accel. Beams*, vol. 28, no. 7, p. 074402, 2025. doi:10.1103/kwxj-4bff

[6] C.-Y. Tsai, "Study of the longitudinal multibunch multiturn collective dynamics in the laser modulators of a steady-state microbunching storage ring: a macroparticle model", *Nuclear Instruments and Methods in Physics Research Section A: Accelerators, Spectrometers, Detectors and Associated Equipment*, vol. 1083, p. 171127, 2026. doi:10.1016/j.nima.2025.171127

[7] Y. Dai, Z. Liu, T. Li, X. Deng, and L. Yan, "Longitudinal beam instability driven by coherent radiation in an SSMB laser modulator", 2026, doi:10.48550/arXiv.2604.27036, arXiv: 2604.27036 [physics.acc-ph],

[8] A. E. Siegman, *Lasers*. Mill Valley, CA, USA: University science books, 1986.

[9] A. Gover, "Superradiant and stimulated-superradiant emission in prebunched electron-beam radiators. i. formulation", *Phys. Rev. ST Accel. Beams*, vol. 8, no. 3, p. 030701, 2005. doi:10.1103/PhysRevSTAB.8.030701

[10] A. W. Chao, *Physics of collective beam instabilities in high energy accelerators*. New York, NY, USA: John Wiley & Sons, Inc., 1993.

[11] A. W. Chao, *Lectures on accelerator physics*. New Jersey, USA: World Scientific, 2020. doi:10.1142/12004

[12] H. Kogelnik and T. Li, "Laser beams and resonators", *Appl. Opt.*, vol. 5, no. 10, pp. 1550–1567, 1966. doi:10.1364/AO.5.001550

[13] X. Deng, *Theoretical and experimental studies on steady-state microbunching*. Springer Nature, 2024. doi:10.1007/978-981-99-5800-9

[14] X. Liu *et al.*, "Prototype optical enhancement cavity for steady-state microbunching", *Review of Scientific Instruments*, vol. 95, no. 10, p. 103004, 2024. doi:10.1063/5.0222951